ACS Catalysis

Research Article

pubs.acs.org/acscatalysis

Zinc-Rich Copper Catalysts Promoted by Gold for Methanol Synthesis

Oliver Martin,[†] Cecilia Mondelli,[†] Daniel Curulla-Ferré,[‡] Charlotte Drouilly,[‡] Roland Hauert,[§] and Javier Pérez-Ramírez*[,†]

[†]Institute for Chemical and Bioengineering, Department of Chemistry and Applied Biosciences, ETH Zurich, Vladimir-Prelog-Weg 1, CH-8093 Zurich, Switzerland

[‡]Total Research & Technology Feluy, Zone Industrielle Feluy C, B-7181 Seneffe, Belgium

[§]Empa, Swiss Federal Laboratories for Materials Science and Technology, Überlandstrasse 129, CH-8600 Dübendorf, Switzerland

Supporting Information

ABSTRACT: In this study, we gathered further understanding of the function of the components in the Cu-ZnO-Al_2O_3 catalyst for methanol synthesis from mixed syngas feeds ($CO/CO_2/H_2$) to rationally develop systems displaying superior performance. In order to unravel the role of ZnO in the hydrogenation of the preferred methanol source, CO_2, and in the (reverse) water−gas shift ((R)WGS) reaction, we tested coprecipitated materials with variable surface zinc content under industrially relevant conditions (5.0 MPa, 503−543 K). We found that a surface enrichment in zinc leads to higher activity and selectivity due to (*i*) the enhancement of the unique synergistic Cu-ZnO interactions boosting CO_2 hydrogenation, (*ii*) the inhibition of the RWGS reaction which produces the undesired CO, and (*iii*) the electronic stabilization of the Cu sites against reoxidation by CO_2 or H_2O. Thus, a catalyst with a surface Zn/(Cu + Zn) ratio of 0.8 displayed superior catalytic properties than a commercial benchmark sample, which featured only half of the ratio. An even more performing catalyst was obtained utilizing oxalates instead of hydroxycarbonates as precursors. The better thermal degradation of the former minimizes the content of residual carbon on the surface of the activated catalyst improving the amount of Cu-ZnO contacts. The retention of the metallic state of copper was greatly favored by the deposition of an electron-withdrawing metal such as gold. The Cu-based activity in mixed syngas and CO_2 hydrogenation of the zinc-rich gold-promoted catalyst was ca. 2 and 4 times higher, respectively, than that of the commercial system.

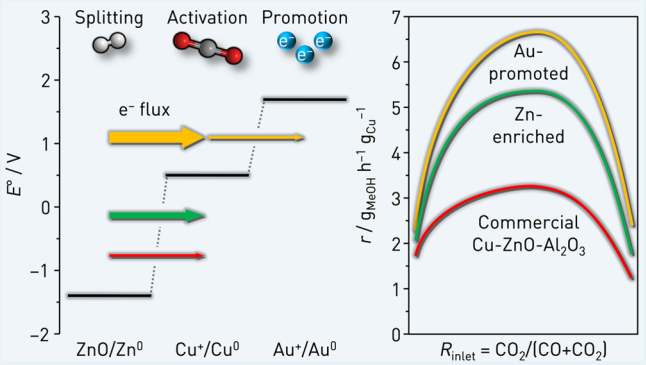

KEYWORDS: *methanol synthesis, (reverse) water−gas shift, Cu-ZnO-Al_2O_3, Cu−Zn synergism, oxalate precursor, gold promotion*

1. INTRODUCTION

Methanol (MeOH) is prospected to play a prominent role in our future economy replacing fossil fuels as a means of energy storage, ground transportation fuel, and platform chemical for synthetic hydrocarbons and their products.[1−4] The standard methanol synthesis process converts syngas over a ternary Cu-ZnO-Al_2O_3 catalyst under high pressures (5.0−10.0 MPa) and elevated temperatures (473−573 K).[5,6] Although it can be operated at variable feed CO/CO_2 ratios, only small CO_2 concentrations are currently applied due to the thermodynamically less favored CO_2 hydrogenation. However, it is well-known that CO_2 positively impacts the kinetics of the reaction.[7] Understanding the role of CO_2 in the mechanism in correlation with the complex structure of the catalysts is thus instrumental to further improve the current technology.

Several studies based on kinetic investigations,[8−12] isotopic labeling,[13−15] and theoretical calculations[16−18] claimed the preferred transformation of CO_2 vs CO into MeOH.[5] However, at small concentrations of CO_2 in the feed, the methanol production rates significantly exceed the sum of the individual rates of CO and CO_2 hydrogenation.[12] It has been highlighted that the concomitant water−gas shift (WGS) reaction ($CO + H_2O \leftrightarrows CO_2 + H_2$) plays a key role in this respect.[19,20] The drop in the rate of methanol formation at high CO_2 concentrations has been initially attributed to an excessive oxygen coverage on the catalyst surface.[21,22] Later investigations indicated that the strong adsorption of the H_2O byproduct on the active sites is the main reason for this inhibition.[9,23,24]

Considering the complex structural and electronic promotion exerted by both ZnO and Al_2O_3 on the copper phase,[25] univocal property-performance correlations are difficult to

Received: April 28, 2015
Revised: August 14, 2015
Published: August 18, 2015

DOI: 10.1021/acscatal.5b00877
ACS Catal. 2015, 5, 5607−5616

establish. The dynamic changes in morphology and surface composition occurring under reaction conditions represent an additional complexity.[19,21,26−28] Beside for its excellent ability to maintain copper particles highly dispersed,[29,30] zinc oxide has demonstrated as an essential ingredient to achieve reasonable CO_2 hydrogenation rates.[31] In this context, it has been proposed that it can either serve as cocatalyst[32,33] or enable the formation of special catalytic sites at its interface with copper[34,35] or that of Cu−Zn alloys.[36−39] Early studies have identified 0.5 and 2.0 as the optimal molar bulk Cu:Zn ratios for binary Cu-ZnO[40] and ternary Cu-ZnO-Al_2O_3[41] systems, respectively. The latter ratio comprises that commonly used in commercial catalysts.[42] However, the catalyst surface properties determining this empirical composition−performance correlation have not been systematically investigated.

Herein, we present the rationalized design of a zinc-rich copper catalyst promoted by gold for methanol synthesis from CO_2-containing syngas. Our approach comprised the preparation of a battery of coprecipitated Cu-ZnO-Al_2O_3 catalysts featuring different bulk Cu:Zn ratios and the measurement of their activity in methanol formation and in the WGS reaction as a function of $R = CO_2/(CO + CO_2)$ at 5.0 MPa, 503−543 K, variable levels of conversion, and H_2O cofeeding. The information gathered in these experiments on the kinetics of the reactions was correlated to the content of zinc and of reduced copper species at the catalyst surface. On the basis of the finding that a higher zinc content enhances the beneficial Cu-ZnO interactions, we regarded that the electronic interplay between these phases, essential for CO_2 hydrogenation, could be hampered by the residual carbon species deriving from the incomplete degradation of the hydroxycarbonate precursor. Therefore, a zinc-rich catalyst was alternatively synthesized from the more easily decomposed oxalates. Finally, we investigated the effect of adding gold to the optimized material because the electron-withdrawing properties of this noble metal should favor the stabilization of metallic copper species. The superior performance of this catalyst compared to that of a commercial benchmark system was demonstrated in a 100 h run.

2. EXPERIMENTAL SECTION

2.1. Catalyst Preparation. A commercial pelletized Cu-ZnO-Al_2O_3 methanol synthesis catalyst possessing a typical metal molar composition Cu:Zn:Al = 6:3:1 was purchased from Alfa Aesar-Johnson Matthey ("copper-based methanol synthesis catalyst", denoted as CuZnAl-2-C). Three Cu-ZnO-Al_2O_3 ternary catalysts with molar Cu:Zn = 0.1, 0.5, and 2 (denoted as CuZnAl-0.1, 0.5, or 2, respectively) and two binary Cu−Al_2O_3 (CuAl) and ZnO-Al_2O_3 (ZnAl) catalysts featuring the same relative content of metals as the commercial material were prepared via coprecipitation. The synthesis comprised the mixing under vigorous stirring of a 1 M aqueous solution containing $Cu(NO_3)_2{\cdot}3H_2O$ (Sigma-Aldrich, 98%), $Zn(NO_3)_2{\cdot}6H_2O$ (Acros Organics, 98%), and/or $Al(NO_3)_3{\cdot}9H_2O$ (Alfa Aesar, 98%) in the desired molar ratio with a 1 M aqueous solution containing the precipitating agent, Na_2CO_3 (Acros Organics, 99.8%), reaching a final pH of 8 of the slurry. The obtained precipitates were filtered without aging, washed with deionized H_2O until the filtrate had pH 7, dried at 338 K overnight, and calcined in static air at 573 K (2 K min^{-1}) for 2 h. In addition to these hydroxycarbonate-derived materials, an oxalate-based catalyst with molar Cu:Zn = 0.5 (denoted as CuZnAl-0.5-OX) was synthesized according to the procedure by Deng et al.[12] Briefly, a 1 M ethanol (Sigma-Aldrich, 99.8%) solution of the above-mentioned Cu, Zn, and Al salts (molar Cu:Zn:Al = 3:6:1) and a 2 M ethanol solution of oxalic acid (Sigma-Aldrich, 99%) were mixed in the volumetric ratio of 1.0:1.2. The obtained gel was filtered directly, washed with 6 L of ethanol, dried, and calcined as described above. The gold-containing catalyst (denoted as CuZnAuAl-0.5-OX) was prepared ad-mixing $HAuCl_4{\cdot}3H_2O$ (abcr, 99.99%) with the metal salt solution resulting in a molar ratio of Cu:Zn:Al:Au = 3:6:1:0.04 (1 wt % Au). The coprecipitation, filtration, drying, and calcination of this material followed the method described above. The activation of all catalysts was performed *in situ* in the catalytic reactor (*vide infra*).

2.2. Characterization. The metal composition of the calcined samples was determined by X-ray fluorescence (XRF) using an Orbis Micro-EDXRF spectrometer equipped with a Rh source (15 kV, 500 μA) and with a silicon drift detector. Powder X-ray diffraction (XRD) was performed using a PANalytical X'Pert Pro MPD utilizing Cu Kα radiation (λ = 0.1542 nm), an angular step size of 0.033° 2θ, and a counting time of 8 s per step. The average particle size of the reduced copper phase was estimated from the Cu(111) reflection applying the Scherrer equation. Nitrogen sorption at 77 K was carried out using a Micromeritics TriStar II instrument. Prior to the measurement, the samples were evacuated at 573 K for 3 h. The total surface area was determined applying the BET equation. Temperature-programmed reduction with hydrogen (H_2-TPR) was carried out in a Thermo TPDRO 1100 instrument. The samples were heated to 623 K (5 K min^{-1}) in a He flow and then exposed to a mixture of 5 mol % H_2/N_2 at this temperature for 1 h to ensure complete reduction of the sample. The catalyst surface was subsequently reoxidized at 323 K in a flow of 1 mol % N_2O/He for 1 h. Finally, the gas flow was switched back to diluted H_2 and the temperature was raised to 623 K (2 K min^{-1}). The copper surface area (S_{Cu}) was calculated according to the method by Gervasini and Bennici[43] applying eq 1

$$S_{Cu} = \frac{n_{H_2} \nu N_A}{C_M W_{cat}} \quad (1)$$

where n_{H_2} is the amount of moles of hydrogen consumed in the TPR experiment after reoxidation of the catalyst surface by N_2O at 323 K and determined by integration of the calibrated TPR signal, ν is the stoichiometric factor (= 2), N_A is the Avogadro constant, C_M is the mean number of copper atoms per m^2 (= 1.40 × 10^{19} m^{-2}), and W_{cat} is the weight of the catalyst.

X-ray photoelectron spectroscopy (XPS) was conducted using a Physical Electronics (PHI) Quantum 2000 X-ray photoelectron spectrometer featuring monochromatic Al Kα radiation, generated from an electron beam operated at 15 kV and 32.3 W, and a hemispherical capacitor electron-energy analyzer equipped with a channel plate and a position-sensitive detector. The samples were extracted from the reactor in a glovebox without passivation and kept under N_2 atmosphere until they were firmly pressed onto indium foil patches, which were then mounted onto a sample platen and introduced into the spectrometer. Our previous study demonstrated that the short exposure to air during this procedure does not cause detectable copper oxidation.[19] The analysis was conducted at 2 × 10^{-7} Pa, with an electron takeoff angle of 45°, and operating the analyzer in the constant pass energy mode. Elemental

DOI: 10.1021/acscatal.5b00877
ACS Catal. 2015, 5, 5607−5616

concentrations were calculated from the photoelectron peak areas after Shirley background subtraction and applying the built-in PHI sensitivity factors. The Auger signals were used to semiquantitatively determine the valence state of Cu. Scanning electron microscopy (SEM) and energy-dispersive X-ray spectroscopy (EDXS) imaging was performed using an aberration-corrected Hitachi HD-2700CS (200 kV) microscope, and high-resolution transmission electron microscopy (HR-TEM) was conducted using an FEI Talos (200 kV) instrument. Samples were prepared depositing a droplet of a suspension of the powders in ethanol on a carbon film supported on a Cu grid.

2.3. Catalytic Evaluation. The catalyst performance was evaluated using a homemade fixed-bed reactor setup (Figure S1 in the Supporting Information) enabling operation under industrial methanol synthesis conditions, i.e., $T \leq 573$ K, $P \leq 10.0$ MPa. The unit consists of a gas (CO, H_2, CO_2, and Ar, Messer, ≥ 99.997%) feeding system equipped with EL-Flow Bronkhorst mass flow controllers and a gas trap containing soda lime (abcr) and a molecular sieve (0.3 nm, Sigma-Aldrich) to remove traces of H_2O or CO_2 present in CO, H_2, and Ar, an high-performance liquid chromatography (HPLC, Gilson 307) pump for liquid injection connected to the heated part on top of the reactor, a reactor (0.65 cm i.d.) made of nickel-lean steel to avoid formation of toxic, volatile nickel tetracarbonyl species, equipped with a thermocouple placed in the reactor wall adjacent to the catalytic bed, and heated by an oven, and an online gas chromatograph (GC) connected through a piping heated to 433 K to prevent condensation.

The undiluted catalyst (0.4 g, particle size = 0.125−0.300 mm) was loaded in the reactor and activated *in situ* through drying at 433 K (2 K min^{-1}) for 30 min in an Ar flow and subsequent reduction at 503 K (2 K min^{-1}) for 2 h in 5 mol % H_2/Ar at a total pressure of 0.5 MPa. Thereafter, the desired methanol synthesis conditions were applied, typically, 503 or 543 K, a total pressure of 5.0 MPa, a molar gas composition of H_2:CO_x:Ar = 4:1:1.5 (CO_x = CO + CO_2), and a total volumetric flow of F_{total} = 130 mL STP min^{-1}. These conditions ensured working below thermodynamic limitation and led to CO_x conversion levels between 5 and 45% depending on the CO_2 content in the syngas and the nature of the catalyst. The concentration of CO_2 in the feed was defined as R = (CO_2/CO_x) × 100%. In tests at a fixed syngas composition of R = 100%, the catalyst was operated at 503 K for 6 h before the temperature was increased to 543 at 2 K min^{-1} and hold for additional 6 h. In cycle experiments, the CO_2 concentration was stepwise increased from R = 0 to 100% and subsequently back to 0% at 503 or 543 K maintaining each step for 6 h. For the determination of the intrinsic reaction rates, experiments were conducted at higher space velocity adjusting the conversion of CO_x to ∼1%, i.e., applying 0.01 g of catalyst at 503 or 543 K, respectively. These conditions were also used for the H_2O cofeeding experiments employing a molar H_2O:CO_x ratio of either 0.3 or 1.0 (F_{total} = 150 mL STP min^{-1}). The WGS reaction was studied under the same conditions using a gas stream (F_{total} = 70 mL STP min^{-1}) of molar composition CO:H_2O:Ar = 1:1:1.5. After each reaction, the catalyst was passivated by flushing with 2 mol % O_2/N_2 at 323 K for 1 h.

Analysis of the outlet gas stream was carried out using an Agilent 7890A GC equipped with a GS-CARBONPLOT column for separating CO, CO_2, Ar, and H_2 coupled to a thermal conductivity detector (TCD) and a DB-1 column to analyze all organic compounds by a flame ionization detector (FID). The time delay between the change at the mass flow controllers and the detection in the GC was ∼30 min. Conversion, yield, rate of product formation, and selectivity were calculated according to equations S1−5 in the Supporting Information. An equilibration time of 6 h was generally found to be sufficient for obtaining constant reaction rates. The carbon balance was determined for each experiment to be ≥95%. All catalysts performed with a selectivity of methanol >98% in terms of organic products under all conditions applied. Dimethyl ether and methyl formate were detected as byproducts only in the conversion of syngas with compositions $0 \leq R \leq 12\%$ over the commercial catalyst. The relative uncertainty of the formation rate of MeOH has been estimated from an error propagation calculation to be 5% on average. All catalytic tests were reproducible within this error range. Mass transfer limitations and channeling were excluded based on dedicated diagnostic experiments which are summarized in Tables S3−5 in the Supporting Information.

3. RESULTS AND DISCUSSION

3.1. Carbon Source and the Role of H_2O in Methanol Synthesis. Recently, we developed an approach to analyze CO_x hydrogenation in a cycle experiment, i.e., progressively increasing the CO_2 concentration (R = CO_2/(CO + CO_2)) in the syngas mixture.[19] If a constant amount of steam is added during this test, the (reverse) water−gas shift ((R)WGS) reaction can be simultaneously evaluated. Herein, we initially applied this method to study a coprecipitated material (CuZnAl-2) featuring a similar bulk composition to a commercial methanol synthesis catalyst (CuZnAl-2-C). Both samples showed a maximum methanol formation at low R values in the cycle experiment without water cofeeding (Figure 1). However, the self-prepared catalyst displayed an almost 3

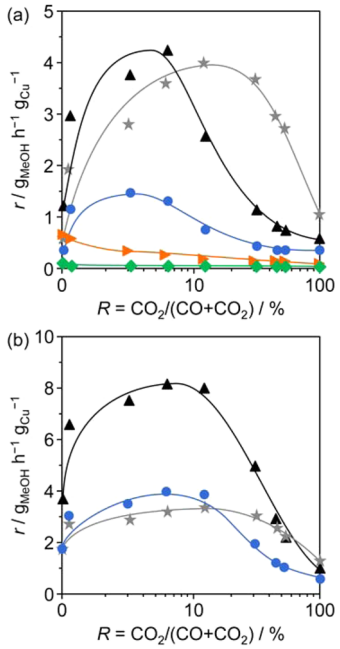

Figure 1. Rate of methanol formation per gram of copper as a function of the CO_2 concentration in the feed at (a) 503 and (b) 543 K over (green ♦) CuAl, (gray ★) CuZnAl-2-C, (blue ●) CuZnAl-2, (▲) CuZnAl-0.5, and (orange ▶) CuZnAl-0.1. Other conditions: P = 5.0 MPa, $GHSV$ = 15 000 h^{-1}, H_2:CO_x = 4, and X_{CO_x} = 5−45%.

DOI: 10.1021/acscatal.5b00877
ACS Catal. 2015, 5, 5607−5616

times lower activity at 503 K (1.5 vs 4.0 g_{MeOH} h^{-1} g_{Cu}^{-1} at the maximum). This result is surprising in view of the similar copper particle size and accessible copper surface area in the two materials before and after the reaction (Table S2 in the Supporting Information). We therefore excluded a major influence of the particle size on the performance. Karelovic and Ruiz[44] have recently reported that the turnover frequency of CO_2 hydrogenation (at 433−498 K and 0.7 MPa) changes with the copper particle size; however, their particles were significantly larger (>25 nm) than the ones applied in our study (5−11 nm). The preparation of the commercial catalyst, which is not disclosed, might have also included an aging step which could determine peculiar surface properties at the basis of its superior catalytic performance.

In order to link the effects observed under industrial conditions with the intrinsic kinetics of the individual reactions, the CO_x conversion was limited to ∼1% by increasing the space velocity. This enables to decouple the (R)WGS reaction from the hydrogenation of CO and CO_2. The cycle experiment conducted at 503 K and in the absence of H_2O over CuZnAl-2-C (Figure 2) indicated that the rate of CO_2 hydrogenation is ca.

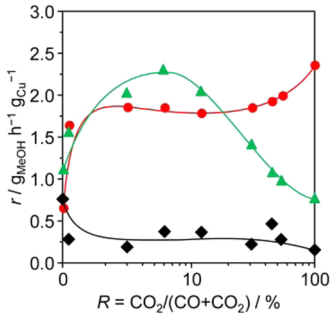

Figure 2. Rate of methanol formation as a function of the CO_2 concentration in the feed over CuZnAl-2-C at GHSV = 600 000 h^{-1} while cofeeding a fixed amount of water, i.e., H_2O:CO_x = (red ●) 0, (green ▲) 0.3, and (black ♦) 1, respectively. Other conditions: T = 503 K, P = 5.0 MPa, H_2:CO_x = 4, and X_{CO_x} ∼ 1%.

4 times higher than that of CO hydrogenation (2.3 vs 0.6 g_{MeOH} h^{-1} g_{Cu}^{-1}), in accordance with Studt, Behrens et al.[45] At R = 1%, almost no CO_2 was detected in the outlet stream (Figure S2 in the Supporting Information), which corroborates that CO_2 is the main carbon source of methanol in CO_2-containing syngas mixtures.

One would expect a linear increase of the methanol formation rate upon elevating R from 0 to 100%. However, the volcano shape of the activity plot at small space velocities (Figure 1) points to self-inhibition by water formed via CO_2 hydrogenation and RWGS. In this respect, Kung et al.[46] suggested that H_2O may strongly adsorb on the catalyst surface blocking the active sites for CO_2 hydrogenation. This is supported by the complete depletion of the catalyst activity in the presence of high concentrations of cofed water (molar H_2O:CO = 1, Figure 2). When applying a smaller H_2O:CO ratio (0.3), the methanol formation rate at R = 6% rose to the same level as observed for R = 100% in the experiment without water cofeeding, but lower rates were observed at higher CO_2 concentrations (0.8 vs 2.3 g_{MeOH} h^{-1} g_{Cu}^{-1}). Sintering of the copper particles was excluded as the reason for the drop in activity at high feed CO_2 contents and low space velocities. Indeed, the catalytic data collected upon decreasing R from 100 to 0% resulted again in a volcano-type plot at slightly lower rates.[19] These results substantiate the generally accepted mechanism in which CO is first converted into CO_2 and subsequently hydrogenated to methanol.[19,20,23]

3.2. Superiority of Zinc-Rich Catalysts. The reason why the maximum methanol formation rates exceed the sum of the CO and CO_2 hydrogenation rates (e.g., 4.0 vs 0.7 + 2.3 g_{MeOH} h^{-1} g_{Cu}^{-1} for CuZnAl-2-C) remains unclear. It is very likely related to the controversially debated[27,32,33,47,48] synergistic interaction between Cu and ZnO, which appears highly sensitive toward the syngas composition. In this regard, Hansen et al.[27] have suggested the formation of specific copper active sites stabilized by ZnO, while Polarz, Hinrichsen et al.[32] and Fink, Hinrichsen et al.[33] have proposed the direct involvement of ZnO as a cocatalyst. In order to gather a deeper understanding of this crucial aspect and possibly further optimize the catalyst formulation, we prepared and tested coprecipitated catalysts featuring the same Al content but different bulk Cu:Zn ratios (CuAl, CuZnAl-2, CuZnAl-0.5, and CuZnAl-0.1, Table 1). Plotting the space-time yield determined at R = 12% in the cycle experiments (Figure 1) vs the copper content in the bulk of the various catalysts unveiled a maximum at Cu/(Cu + Zn) = 0.35 (Figure 3a). This result is in contrast to literature data[41] evidencing a maximum at much higher copper concentrations (Cu/(Cu + Zn) = 0.80, Figure 3b) for Cu-ZnO-Al_2O_3 catalysts. The latter value is similar to that found for CuZnAl-2-C. Klier et al.[40] have studied binary Cu-ZnO catalysts under similar conditions and found the composition Cu/(Cu + Zn) = 0.30 optimal, thus being in

Table 1. Characterization Data of the Catalysts

catalyst	Cu[a] (wt %)	Zn[a] (wt %)	Al[a] (wt %)	molar Cu:Zn:Au:Al[a] (−)	molar Zn/(Cu+Zn)[b] (−)	molar $Cu^0/(Cu^+ + Cu^0)$[c] (−)	C[b] (at.%)	S_{Cu}[d] (m^2 g^{-1})	D_{Cu}[e] (nm)	d_{pore}[f] (nm)
CuZnAl-2-C[g]	50.6	22.5	4.6	6.0:2.6:1.3	0.51	0.15	12.7	24.0 ± 0.4	6.0 ± 0.7	13
CuZnAl-2	48.3	27.3	2.9	6.0:3.3:0.9	0.35	0.05	12.5	25.6 ± 0.3	8.0 ± 0.6	16
CuZnAl-0.5	23.3	52.6	2.9	3.0:6.6:0.9	0.74	0.39	10.5	23.5 ± 0.5	4.8 ± 0.9	30
CuZnAl-0.5-OX[h]	25.8	53.5	0.6	3.0:6.0:0.2	0.83	0.66	5.6	11.1 ± 0.7	7.4 ± 0.6	16
CuZnAuAl-0.5-OX[i]	23.0	52.0	3.1	3.0:6.6:0.06:0.6	0.90	0.89	4.0	15.9 ± 0.5	6.8 ± 0.8	20
CuZnAl-0.1	6.6	70.5	2.1	0.9:9.4:0.7	0.95	n.a.[j]	14.4	4.8 ± 1.4	6.9 ± 0.6	30
CuAl	73.2	–	4.4	6.0:0:0.9	0.00	0.01	–	21.3 ± 0.5	11.1 ± 0.5	46
ZnAl	–	50.2	19.9	0:3.0:2.9	1.00	–	–	–	–	–

[a]XRF. [b]XPS. [c]AES. [d]H_2-TPR after oxidation of the activated catalysts by N_2O at 323 K. [e]Derived from the XRD pattern of the activated catalyst. [f]Average pore diameter from the BJH method. [g]Commercial catalyst. [h]Prepared using oxalate salts as precursors. [i]1.4 wt % of Au was introduced upon precipitation of the catalyst. [j]Signal was too low for a reliable evaluation.

DOI: 10.1021/acscatal.5b00877
ACS Catal. 2015, 5, 5607−5616

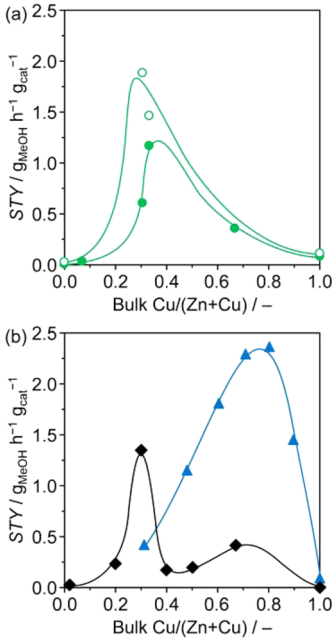

Figure 3. (a) Space-time yield of methanol as a function of the bulk copper content in Cu-ZnO-Al_2O_3 catalysts applied in this study at (green ●) 503 and (green ○) 543 K. Other conditions: P = 5.0 MPa, $GHSV$ = 15 000 h^{-1}, H_2:CO_x = 4.0, and R = 12%. (b) Corresponding literature data for (black ◆) Cu-ZnO catalysts[40] (T = 523 K, P = 7.5 MPa, GHSV = 5,000 h^{-1}, H_2:CO_x = 2.3, and R = 20%) and (blue ▲) Cu-ZnO-Al_2O_3 catalysts[41] (T = 495 K, P = 6.7 MPa, H_2:CO_x = 7.6, and R = 11%).

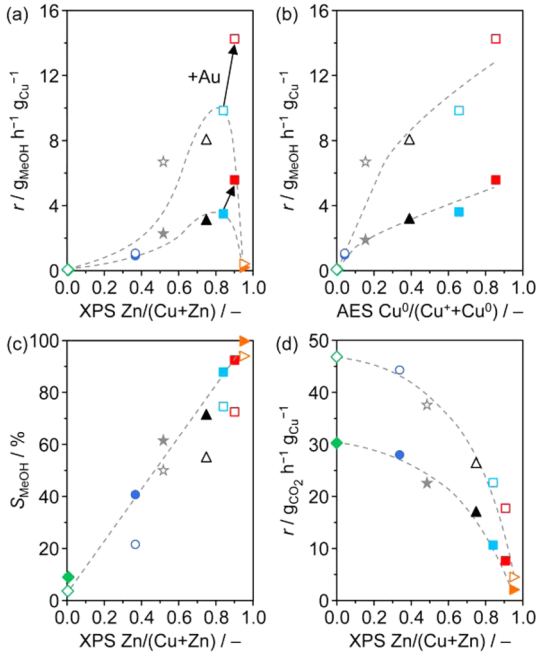

Figure 4. Rate of methanol formation via CO_2 hydrogenation as a function of (a) the zinc content and (b) the concentration of Cu^0 species at the surface of the used catalysts. Conditions: P = 5.0 MPa, GHSV = 600 000 h^{-1}, H_2:CO_2 = 4, and X_{CO_2} ∼ 1%. (c) Methanol selectivity in CO_2 hydrogenation as a function of the surface zinc content. (d) Rate of CO_2 formation via the WGS reaction as a function of the surface zinc content. Conditions: P = 5.0 MPa, GHSV = 240 000 h^{-1}, H_2O:CO = 1, and X_{CO} ∼ 1%. (gray ★, ☆) CuZnAl-2-C, (blue ●, ○) CuZnAl-2, (black ▲, △) CuZnAl-0.5, (turquoise ■, □) CuZnAl-0.5-OX, (red ■, □) CuZnAuAl-0.5-OX (orange ▶, ▷) CuZnAl-0.1, and (green ♦, ◊) CuAl. Solid and open symbols refer to the data collected at 503 and 543 K, respectively.

line with the data for our ternary systems. These discrepancies could stem from the application of a different temperature (363 vs 298 K) upon the synthesis. Schüth et al.[49] have shown that this parameter significantly affects the bulk properties of the resulting catalysts. Their surface compositions are expected to strongly vary as well. Unfortunately, this aspect was not analyzed in the works cited. Furthermore, the reported space-time yields do not decouple CO_2 hydrogenation from the WGS reaction. Consequently, we better correlated the rates of CO_2 hydrogenation and WGS at high space velocity with the relative surface zinc content in the used catalysts, expressed as Zn/(Cu + Zn) (Figures 4a,d). The curve for the CO_2 hydrogenation rate (Figure 4a) displays a volcano-type shape, which is more pronounced at 543 than 503 K. The highest rates were exhibited by CuZnAl-0.5. While the copper surface area of this catalyst is similar to that of CuZnAl-2 (23.5 vs 25.6 m^2 g^{-1}, Table 1), it featured smaller copper particles (4.8 vs 8.0 nm) and an enhanced surface Zn/(Cu + Zn) ratio (0.74 vs 0.35). Both properties are likely associated with an improved interaction between Cu and ZnO and thus explain its superior performance in CO_2 hydrogenation (Figure 4a) and the cycle experiment (Figure 1). The linearly decreasing rather than volcano-type shape of the methanol formation rate at variable R over CuZnAl-0.1 (Figure 1) was attributed to the excessive surface concentration of Zn, which reduces the copper sites available for CO_2 hydrogenation.

Some studies have recently demonstrated the positive impact by ZnO on the copper phase with respect to both activity and selectivity in methanol synthesis. Le Valant, Comminges et al.[50] have reported a 100% selective core−shell catalyst, i.e., ZnO_x deposited on Cu powder. This material featured 3 times higher methanol formation rates from CO_2 compared to a conventional coprecipitated Cu-ZnO sample (Cu:Zn = 0.4 in the bulk). Unfortunately, those results were not correlated with the surface composition of the samples. Willinger et al.[51] have claimed a positive contribution by surface ZnO_x layers which are formed as soon as the catalyst is exposed to syngas under reaction conditions. In line with these results, we identified a significant surface enrichment of Zn in the highly active catalysts, i.e., CuZnAl-2-C and CuZnAl-0.5 (Figure S3 in the Supporting Information). On the basis of the similar bulk Al content in all of the samples studied but their significantly different surface Zn concentration, we claim that alumina plays a negligible role in determining the migration of Zn to the surface. In addition to the creation of the active sites at the Cu-ZnO interface, the different Cu:Zn ratios in the bulk may also influence the relative amount of copper facets exposed, which possess different intrinsic activity for CO_2 hydrogenation.[17]

The zinc concentration of the catalyst surface also impacts the (R)WGS activity. The monotonic increase of the methanol selectivity in CO_2 hydrogenation with rising surface Zn/(Cu + Zn) values indicates lower RWGS reaction rates over zinc-rich catalysts (Figure 4c). This is in accordance with the results gathered by Nakamura et al.[52] with Zn vapor-deposited over Cu(111) single crystals. An efficient suppression of the RWGS limits the inhibitory effect of water on the methanol formation rate. No CO is formed in CO_2 hydrogenation at a high space velocity (Figure S2 in the Supporting Information), revealing that the RWGS reaction generally proceeds with much lower

DOI: 10.1021/acscatal.5b00877
ACS Catal. 2015, 5, 5607−5616

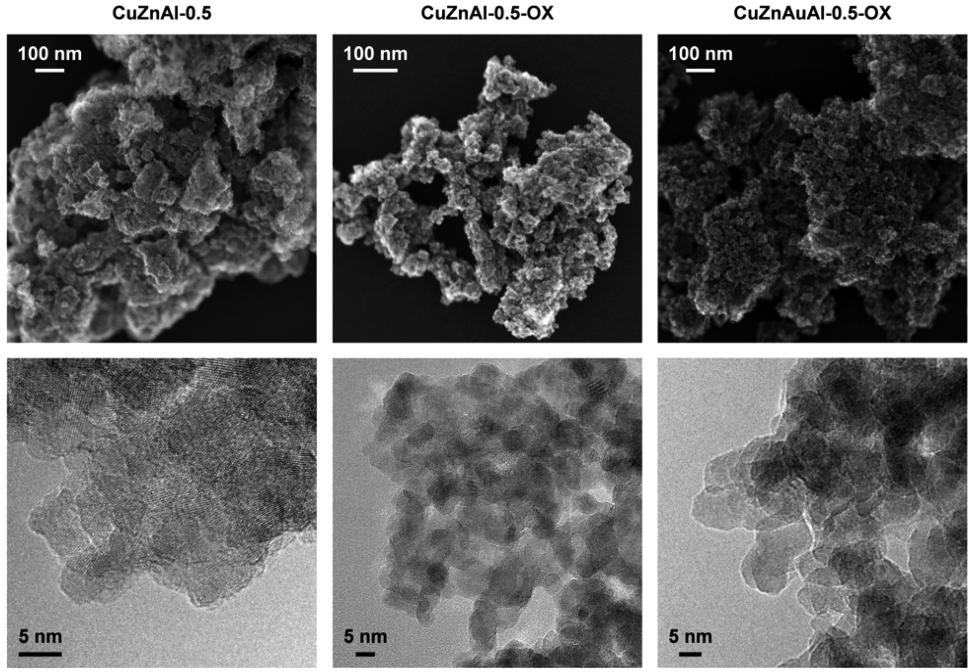

Figure 5. SEM (top row) and HR-TEM (bottom row) of the zinc-rich catalysts after the CO cycle (T = 543 K, P = 5.0 MPa, $GHSV$ = 15 000 h^{-1}, H_2:CO_x = 4, and X_{CO_x} = 5−45%).

rates than the WGS reaction and CO_2 hydrogenation which is expected from the thermodynamic equilibrium. This explains the higher sensitivity of the RWGS toward the surface zinc concentration compared to the WGS (Figure 4d) and that, among the ternary samples, only the CuZnAl-0.1 catalyst did not display a maximum of the methanol formation rate in the cycle experiment (Figure 1). Additionally, the rates of the WGS reaction (Figure 4d) are much larger than those of CO_2 hydrogenation (Figure 4a). Hence, the WGS reaction is not the limiting step in methanol synthesis. This is corroborated by the fact that a higher amount of CO_2 is present in the outlet gas stream compared to the inlet feed at lower space velocity (Figure S2 in the Supporting Information). Thus, we generally conclude that a good methanol synthesis catalyst is also a good WGS catalyst but not necessarily *vice versa*. Moreover, the absence of the maximum rate in the cycle experiment at high space velocity (Figure 2) suggests that different sites might be active for the (R)WGS and CO_2 hydrogenation. In this respect, Schlögl, Behrens et al.[53] demonstrated through H/D exchange experiments that RWGS and CO_2 hydrogenation do not share a common intermediate. Furthermore, a calorimetric and adsorption study by Ostrovskii[54] indicated that methanol synthesis proceeds over ZnO and the (R)WGS over Cu sites. The low WGS activity and low RWGS selectivity of our zinc-rich catalysts (Figure 4c,d) appear to support these findings.

In order to gain further insights into the interaction between Cu and ZnO, we determined the valence states associated with the surface copper species in the used catalysts by Auger electron spectroscopy (Figure S4 in the Supporting Information). According to their standard reduction potentials, i.e., $E^{\circ}_{Cu^+/Cu}$ = 0.5 V and $E^{\circ}_{ZnO/Zn}$ = −1.3 V, copper should preferably be in metallic state and Zn in oxidic state. While the situation in the real catalyst is far more complex than in a model layered material, the Schottky junction theory introduced by Frost[55] already hypothesized an electronic flux from the semiconductor (ZnO) to the metal (Cu) resulting in a negative charging of the latter. Recently, Calaza et al.[56] have reported that in an Au/MgO system, where the two components are characterized by similar electrochemical properties to the Cu-ZnO pair, electrons are transferred from the oxide to the metal accumulating at the phase boundary. These negatively charged gold atoms appeared as the most active for CO_2 hydrogenation within the material. Accordingly, it is plausible to assume that copper atoms directly in contact with the zinc phase would more easily remain in reduced state, while those which are not adjacent to ZnO might be more easily oxidized by CO_2 or H_2O. Since spillover of protons from ZnO to copper has been proposed in various works,[57] it is likely that the electron flux is compensated by this phenomenon to maintain the charge neutrality in the material. Thus, we supposed that the fraction of surface Cu^0 species can be a qualitative measure of how efficiently Cu and ZnO interact at the catalyst surface. A monotonic increase of the CO_2 hydrogenation rate was observed with ascending values of the surface Cu^0/(Cu^++Cu^0) ratio (Figure 4b), which was the highest for CuZnAl-0.5. The same trend was observed when normalizing the reaction rates to the copper surface area (Figure S5a in the Supporting Information), indicating that CO_2 hydrogenation also depends on the Cu-ZnO contacts and not only on the total amount of Cu sites at the surface. In contrast, a drop in reaction rate was evidenced for the WGS (Figure S5b in the Supporting Information) with increasing surface Zn/(Cu + Zn) ratio, pointing out that ZnO negatively affects the activity of the Cu sites for this reaction. Although our *ex situ* obtained data on the oxidation states do not necessarily reflect the situation of the system at work, our results suggest that (negatively charged) metallic Cu adjacent to ZnO is one of the main active sites in CO_2 hydrogenation. Oppositely, these species might hinder the oxidation of CO to CO_2 upon WGS especially in zinc-rich catalysts. While Frost[55] concluded that the charge transfer from ZnO to Cu creates vacancies in the metal oxide where the hydrogenation of CO_2 exclusively occurs, recent studies point

DOI: 10.1021/acscatal.5b00877
ACS Catal. 2015, 5, 5607−5616

to metallic Cu[16] or Cu-ZnO_x boundaries[25] as the main active site for CO_2 activation without excluding a mechanistic involvement of oxygen vacancies at the metal oxide surface.[17,32,33] These conclusions are in line with our results but in contrast to the hypothesis of Cu−Zn alloying.[39,58] In this respect, we would like to point out that since Cu−Zn intermetallic species are hardly detected by *ex situ* techniques due to their instability, their presence under CO_2-rich syngas conditions is also unprobable as Zn is very likely reoxidized to ZnO. This is supported by a recent *in situ* neutron diffraction investigation of a commercial Cu-ZnO-Al_2O_3 catalyst under mixed syngas (R = 57) at 523 K and 6.0 MPa, i.e., under similar conditions to those used in our study.[59]

3.3. Tuning the Interaction between Cu and ZnO. Hydroxycarbonates, conventionally employed as catalyst precursors, lead to the presence of residual carbonates in the activated material (Table 1), which cannot be removed without irreversibly damaging the active phase. Such carbon deposits might hamper the interaction between Cu and ZnO if located at their phase boundaries. In view of the importance of the Cu-ZnO contacts for CO_2 hydrogenation, we conceived to synthesize the optimized catalyst, i.e., CuZnAl-0.5, alternatively applying the more easily degradable oxalates as precursors. The obtained solid (CuZnAl-0.5-OX) indeed featured a reduced carbon concentration at the surface (5.6 vs 10.5 at. % in CuZnAl-0.5). Its BET surface area and total pore volume were slightly higher with respect to the hydroxycarbonate-derived sample (S_{BET} = 66 vs 54 $m^2\ g^{-1}$, V_{pore} = 0.24 vs 0.21 mL g^{-1}), in line with the smaller particle size observed by electron microscopy (Figure 5). However, the Cu surface area was inferior (11.1 vs 23.5 $m^2\ g^{-1}$). Still, CuZnAl-0.5-OX exhibited much higher surface Zn/(Cu + Zn) and $Cu^0/(Cu^+ + Cu^0)$ ratios (Table 1). Accordingly, it displayed the highest CO_2 hydrogenation rate of all catalysts, which rose from 3.5 to 9.7 $g_{MeOH}\ h^{-1}\ g_{Cu}^{-1}$ increasing the temperature from 503 to 543 K (Figure 4a,b), and the best activity in the cycle experiment (Figure 6a). The maximum methanol formation rate over CuZnAl-0.5-OX occurred at larger R in the cycle compared to the other coprecipitated catalysts, highlighting a higher resistance of the copper sites against reoxidation. This could be proved by H_2-TPR of the used catalysts (Figure 6b). Because ZnO is usually irreducible under the conditions applied in the analysis and the bulk copper phase remained in the metallic state (see XRD in Figure S6 in the Supporting Information), the H_2-TPR profiles collected are exclusively indicative of surface copper species. CuZnAl-0.5, CuZnAl-0.5-OX, and CuZnAl-2-C produced reduction peaks at significantly lower temperatures compared to the other catalysts. Their easier reducibility correlates to the larger fraction of Cu sites in close vicinity to ZnO in these systems and explains their better performance in the cycle experiment.

The concept of electronic interaction between copper and zinc oxide can be extrapolated to catalysts with alternative metal oxides, like ZrO_2 (CuZrAl-2) or CeO_2 (CuCeAl-2). The standard reduction potential of ZrO_2, $E^\circ_{ZrO_2/Zr}$ = −1.6 V, is close to that of ZnO explaining the activity of the zirconia-containing catalyst for methanol synthesis observed by us (Figure S7 in the Supporting Information) and in other studies.[60] However, the poorer ability of this sample to inhibit the RWGS reaction (S_{MeOH} = 18 vs 45% of CuZnAl-2 in CO_2 hydrogenation) does not favor its application for methanol synthesis from mixed syngas feeds. The situation for CeO_2 is

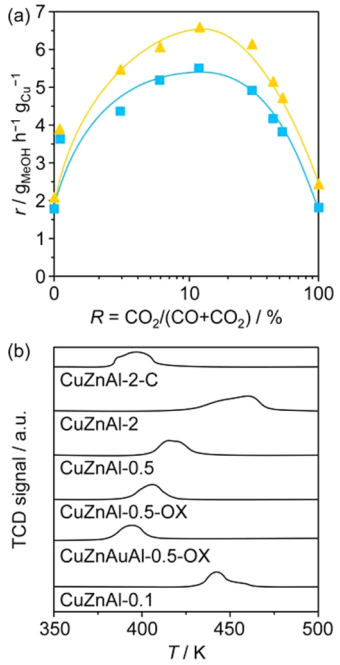

Figure 6. (a) Rate of methanol formation as a function of the CO_2 concentration in the feed over (blue ■) CuZnAl-0.5-OX and (yellow ▲) CuZnAuAl-0.5-OX. Reaction conditions: T = 543 K, P = 5.0 MPa, $GHSV$ = 15 000 h^{-1}, H_2:CO_x = 4, and X_{CO_x} = 5−45%. (b) H_2-TPR profiles of the commercial catalyst, the coprecipitated samples with differing bulk Cu:Zn ratios, and the gold-containing catalyst after the CO cycle at 543 K.

more complex. The standard reduction potential of Ce^{3+}/Ce (−2.3 V) leads to the expectation of an even higher electronic flux from ceria to copper and thus of a greater activity. However, ceria typically comprises Ce^{4+} and Ce^{3+} cations and the standard reduction potential of Ce^{4+}/Ce^{3+} is +1.7 V. Therefore, this oxide will effectively withdraw electrons from the copper phase resulting in a reversed electronic flux compared to the case of Cu-ZnO and Cu-ZrO_2. This is manifested in the very poor methanol formation rate over CuCeAl-2 (Figure S7 in the Supporting Information). The superior activity of a CeO_x/Cu(111) system with respect to Cu particles deposited on Zn(000$\bar{1}$) reported in the study by Rodriguez et al.[61] could be the consequence of different oxidation states of cerium present in their model catalyst with respect to practical samples such as our coprecipitated materials. Furthermore, they claimed to form a highly active interface between the metal and partially reduced metal oxide which might not be reflected in our sample due to the different preparation routes. Other Cu-MO_x-Al_2O_3 (M = Cr, Sn, Ti) catalysts tested in our study did not show significant methanol formation rates. The uniqueness of ZnO might relate to its peculiar transformation from a semiconductor into a conductive material in hydrogen atmospheres,[62] which shall emphasize electronic interactions with the copper phase.

In order to prove the concept of electronic flux between Cu and ZnO and possibly further boost the catalytic performance, gold was exploited as promoter due to its noble character. Because small Au clusters can be active for CO_2 hydrogenation,[63,64] we targeted the introduction of large Au crystallites. The gold precursor was ad-mixed upon the coprecipitation of the CuZnAl-0.5-OX catalyst resulting in a loading of 1 wt % Au (Table 1). The coprecipitation approach

DOI: 10.1021/acscatal.5b00877
ACS Catal. 2015, 5, 5607−5616

was favored over impregnation/deposition methods[63] because the impregnation of CuZnAl-0.5-OX by the gold precursor induced strong sintering of the copper particles upon exposure to water. The catalyst obtained (CuZnAuAl-0.5-OX) featured a significantly higher S_{BET} than CuZnAl-0.5-OX (100 vs 66 $m^2 g^{-1}$). This difference might stem from the influence of the strongly acidic character of the gold precursor ($HAuCl_4$) upon synthesis. XPS did not detect the noble metal at the surface of CuZnAuAl-0.5-OX (detection limit 0.05 at. %), but XRD evidenced the presence of gold in the used catalyst in form of a metallic phase and of intermetallic Cu−Au compounds (Figure S6 in the Supporting Information). EDXS identified large Au particles (~15 nm) in close proximity to Cu clusters (Figure S8 in the Supporting Information). Thus, gold was supposed to electronically interact from the bulk with copper, as schematically shown in Figure 7: the electron-withdrawing

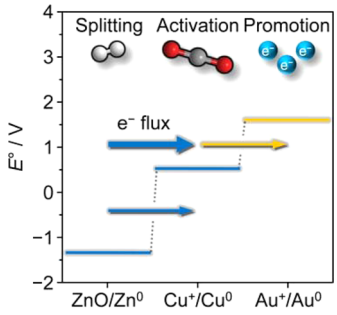

Figure 7. Schematic representation of the promotional effect of gold in CuZnAuAl-0.5-OX on the basis of the standard reduction potentials E° of the individual catalyst components. Owing to its electron-withdrawing properties, gold enhances the electronic flux from ZnO to Cu, favoring the preservation of the metallic state of Cu and thus its activity for CO_2 hydrogenation.

action of Au shall enhance the electronic flux from ZnO to Cu stabilizing Cu^0 species. Indeed, whereas the Zn/(Cu + Zn) ratio for this catalyst was only slightly higher, the $Cu^0/(Cu^+ + Cu^0)$ ratio increased to a greater extent (Table 1) with respect to CuZnAl-0.5-OX. A control experiment with a ZnAl catalyst containing 1 wt % of Au and featuring similar Au particle sizes as in the corresponding Cu-based catalyst showed no activity. Both the CO_2 hydrogenation rate (Figure 4a,b) and the maximum methanol formation rate in the cycle experiment (Figure 6a) were significantly higher over CuZnAuAl-0.5-OX compared to its gold-free analogue. No clear correlation was found for the CO_2 hydrogenation activity with the BET surface area. Therefore, the superiority of the gold-containing catalyst is assumed to mainly originate from the electronic promotion exerted by the noble metal. The latter is further corroborated by the fact that Cu in this sample reduced at lower temperature as shown by the H_2-TPR profiles (Figure 6b).

Compared to the commercial sample, our optimized gold-promoted zinc-rich catalyst displayed an outstanding CO_2 hydrogenation activity at 543 K not only in terms of Cu-based reaction rate (7.1 vs 14.3 $g_{MeOH}\ h^{-1}\ g_{Cu}^{-1}$, Figure 4a) but also of space-time yield (2.1 vs 3.3 $g_{MeOH}\ h^{-1}\ g_{cat}^{-1}$). Therefore, we compared the performance of this promising material and of the commercial system in a 100 h run under fixed industrial-like conditions (Figure 8). No deactivation was observed during this period for either of the materials in agreement with unaltered H_2-TPR profiles recorded after 6 and 100 h time-on-stream. Remarkably, the Cu-based methanol formation rate was

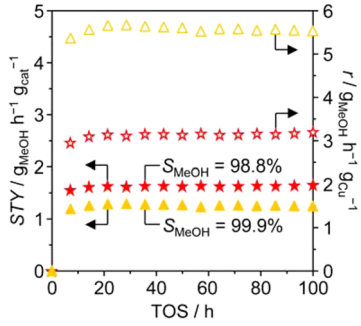

Figure 8. Evolution of the space-time yields (solid symbols) and rate of methanol formation (open symbols) over (red ★, ☆) CuZnAl-2-C (X_{CO_x} = 39%) and (yellow ▲, △) CuZnAuAl-0.5-OX (X_{CO_x} = 30%) in a 100-h catalytic run at T = 543 K, P = 5.0 MPa, $GHSV$ = 15 000 h^{-1}, H_2:CO_x = 4, and R = 12%.

2 times higher over CuZnAuAl-2-OX than over CuZnAl-2-C. Though, the space-time yield over the novel catalyst was inferior by 20%. In this respect, we put forward that its greater CO_2 hydrogenation rate causes a more pronounced inhibitory effect by H_2O. Interestingly, the selectivity to methanol among organic products (methanol, dimethyl ether, and methyl formate) of CuZnAuAl-2-OX was superior to that of the commercial sample (99.9 vs 98.8%). Overall, our optimized catalyst stands as a system of potential interest for methanol synthesis from CO_2-containing syngas.

Our investigations demonstrate the importance of a rationalized catalyst design for methanol synthesis. Further research is still required for elucidating the real active sites in Cu-ZnO-Al_2O_3-based catalysts. We are currently directing efforts to the extremely challenging characterization of the catalyst under reaction conditions as the only enabling strategy to this end. Besides, novel tailor-made catalysts might have to face different syngas compositions than in the current industrial process. In the ongoing development of such materials, one shall consider that under standard fixed-bed reactor conditions the full activity of a catalyst can be hardly exploited because thermodynamics limits the conversion degree down to 5−10% for pure CO_2 hydrogenation. New process concepts[65] are required and have to be designed together with the catalyst in order to adjust the critical amount of water necessary to convert CO into CO_2 and to simultaneously shift the equilibrium of CO_2 hydrogenation for maximizing the one pass conversion.

4. CONCLUSIONS

Herein, we designed a zinc-rich Cu-ZnO-Al_2O_3 catalyst promoted by gold which greatly surpasses the commercial benchmark system in terms of activity and selectivity upon methanol synthesis from mixed syngas feeds ($CO/CO_2/H_2$) and shows a stable behavior in a 100 h catalytic run. A higher surface Zn content inhibited the reverse water−gas shift reaction and led to a greater amount of copper atoms being in close proximity to zinc oxide thus enhancing the resistance of the copper sites toward reoxidation by CO_2 or H_2O. The application of oxalates instead of the conventionally utilized hydroxycarbonates in the preparation of the catalyst was effective in minimizing the amount of carbon at the catalyst surface, fostering a more efficient interaction between Cu and ZnO. The introduction of small amounts of a noble metal like gold significantly promoted the electronic stabilization of Cu^0

DOI: 10.1021/acscatal.5b00877
ACS Catal. 2015, 5, 5607−5616

sites, which appear to be the main active sites in CO_2 hydrogenation.

■ ASSOCIATED CONTENT

Supporting Information

The Supporting Information is available free of charge on the ACS Publications website at DOI: 10.1021/acscatal.5b00877.

Description of the synthesis of the additionally tested Cu-MO_x-Al_2O_3 (M = Ce, Cr, Sn, Ti, Zr) catalysts; formulas used to calculate conversion, yield, selectivity, space-time yield, and rates; bulk composition of the Cu-MO_x-Al_2O_3 catalysts (Table S1); comparison of copper surface area and copper particle size of all catalysts applied (Table S2); assessment of mass transfer limitations and channeling (Tables S3−5); photograph and piping and instrumentation diagram of the miniplant (Figure S1); CO_2 concentration in outlet gas stream vs the one in the syngas feed (Figure S2); surface vs bulk Zn content in the catalysts studied (Figure S3); Cu AES spectra of selected catalysts (Figure S4); reaction rates of CO_2 hydrogenation and WGS normalized by the Cu surface area (Figure S5); X-ray diffraction patterns of used catalysts (Figure S6); CO cycles over Cu-ZrO_2−Al_2O_3 and Cu-CeO_2−Al_2O_3 (Figure S7); EDXS map of the Au-containing catalyst (Figure S8) (PDF)

■ AUTHOR INFORMATION

Corresponding Author

*E-mail: jpr@chem.ethz.ch. Fax: +41 44 633 1405.

Notes

The authors declare no competing financial interest.

■ ACKNOWLEDGMENTS

Total Research & Technology Feluy is acknowledged for sponsoring this research. We thank Dr. K. Hortmann and Dr. A. J. Martín Fernández for fruitful discussions, the Scientific Center for Optical and Electron Microscopy ScopeM for use of their facilities, Dr. F. Krumeich for the electron microscopy studies, and F. Brüning and M. Stummann for experimental input.

■ REFERENCES

(1) Olah, G. A. *Angew. Chem., Int. Ed.* **2005**, *44*, 2636−2639.
(2) Aresta, M. *Carbon Dioxide as Chemical Feedstock*; Wiley-VCH Verlag GmbH & Co. KGaA: Weinheim, 2010; p 394.
(3) Bertau, M.; Offermanns, H.; Plass, L.; Schmidt, F.; Wernicke, H.-J. *Methanol: The Basic Chemical and Energy Feedstock of the Future*; Springer: Heidelberg, 2014; p 677.
(4) Kondratenko, E. V.; Mul, G.; Baltrusaitis, J.; Larrazábal, G. O.; Pérez-Ramírez, J. *Energy Environ. Sci.* **2013**, *6*, 3112−3135.
(5) Lee, S. *Methanol Synthesis Technology*; CRC Press: Boca Raton, 1990; p 236.
(6) Hansen, J. B.; Nielsen, P. E. H. In *Handbook of Heterogeneous Catalysis*, 2nd ed.; Ertl, G., Knözinger, H., Schüth, F., Weitkamp, J., Eds.; Wiley-VCH Verlag GmbH & Co. KGaA: Weinheim, 2008; Vol. *6*, pp 2920−2949.
(7) Klier, K.; Chatikavanij, V.; Herman, R. G.; Simmons, G. W. *J. Catal.* **1982**, *74*, 343−360.
(8) Chinchen, G. C.; Spencer, M. S.; Waugh, K. C.; Whan, D. A. *J. Chem. Soc., Faraday Trans. 1* **1987**, *83*, 2193−2212.
(9) Muhler, M.; Törnqvist, E.; Nielsen, L. P.; Clausen, B. S.; Topsøe, H. *Catal. Lett.* **1994**, *25*, 1−10.
(10) Topsøe, H.; Ovesen, C. V.; Clausen, B. S.; Topsøe, N.-Y.; Højlund Nielsen, P. E. H.; Törnqvist, E.; Nørskov, J. K. In *Dynamics of Surfaces and Reaction Kinetics in Heterogeneous Catalysis*; Froment, G. F., Waugh, K. C., Eds.; Elsevier Science Bv: Amsterdam, 1997; Vol. *109*, pp 121−139.
(11) Yang, Y.; Mims, C. A.; Mei, D. H.; Peden, C. H. F.; Campbell, C. T. *J. Catal.* **2013**, *298*, 10−17.
(12) Zhang, Y. L.; Sun, Q.; Deng, J.; Wu, D.; Chen, S. Y. *Appl. Catal., A* **1997**, *158*, 105−120.
(13) Chinchen, G. C.; Denny, P. J.; Parker, D. G.; Spencer, M. S.; Whan, D. A. *Appl. Catal.* **1987**, *30*, 333−338.
(14) Liu, G.; Willcox, D.; Garland, M.; Kung, H. H. *J. Catal.* **1985**, *96*, 251−260.
(15) Rozovskii, A. Y.; Lin, G. I. *Kinet. Catal.* **1999**, *40*, 773−794.
(16) Grabow, L. C.; Mavrikakis, M. *ACS Catal.* **2011**, *1*, 365−384.
(17) Behrens, M.; Studt, F.; Kasatkin, I.; Kühl, S.; Hävecker, M.; Abild-Pedersen, F.; Zander, S.; Girgsdies, F.; Kurr, P.; Kniep, B.-L.; Tovar, M.; Fischer, R. W.; Nørskov, J. K.; Schlögl, R. *Science* **2012**, *336*, 893−897.
(18) Yang, Y.; Evans, J.; Rodriguez, J. A.; White, M. G.; Liu, P. *Phys. Chem. Chem. Phys.* **2010**, *12*, 9909−9917.
(19) Martin, O.; Pérez-Ramírez, J. *Catal. Sci. Technol.* **2013**, *3*, 3343−3352.
(20) Chanchlani, K. G.; Hudgins, R. R.; Silveston, P. L. *J. Catal.* **1992**, *136*, 59−75.
(21) Peter, M.; Fendt, J.; Pleintinger, S.; Hinrichsen, O. *Catal. Sci. Technol.* **2012**, *2*, 2249−2257.
(22) Saito, M.; Fujitani, T.; Takeuchi, M.; Watanabe, T. *Appl. Catal., A* **1996**, *138*, 311−318.
(23) Lee, J. S.; Lee, K. H.; Lee, S. Y.; Kim, Y. G. *J. Catal.* **1993**, *144*, 414−424.
(24) Sahibzada, M.; Metcalfe, I. S.; Chadwick, D. *J. Catal.* **1998**, *174*, 111−118.
(25) Schumann, J.; Eichelbaum, M.; Lunkenbein, T.; Thomas, N.; Álvarez-Galván, M. C.; Schlögl, R.; Behrens, M. *ACS Catal.* **2015**, *5*, 3260.
(26) Grunwaldt, J.-D.; Molenbroek, A. M.; Topsøe, N.-Y.; Topsøe, H.; Clausen, B. S. *J. Catal.* **2000**, *194*, 452−460.
(27) Hansen, P. L.; Wagner, J. B.; Helveg, S.; Rostrup-Nielsen, J. R.; Clausen, B. S.; Topsøe, H. *Science* **2002**, *295*, 2053−2055.
(28) Wilmer, H.; Hinrichsen, O. *Catal. Lett.* **2002**, *82*, 117−122.
(29) Prieto, G.; Zečević, J.; Friedrich, H.; de Jong, K. P.; de Jongh, P. E. *Nat. Mater.* **2012**, *12*, 34−39.
(30) Kurtz, M.; Wilmer, H.; Genger, T.; Hinrichsen, O.; Muhler, M. *Catal. Lett.* **2003**, *86*, 77−80.
(31) Zander, S.; Kunkes, E. L.; Schuster, M. E.; Schumann, J.; Weinberg, G.; Teschner, D.; Jacobsen, N.; Schlögl, R.; Behrens, M. *Angew. Chem., Int. Ed.* **2013**, *52*, 6536−6540.
(32) Polarz, S.; Strunk, J.; Ischenko, V.; van den Berg, M. W. E.; Hinrichsen, O.; Muhler, M.; Driess, M. *Angew. Chem., Int. Ed.* **2006**, *45*, 2965−2969.
(33) Kurtz, M.; Strunk, J.; Hinrichsen, O.; Muhler, M.; Fink, K.; Meyer, B.; Wöll, C. *Angew. Chem., Int. Ed.* **2005**, *44*, 2790−2794.
(34) García-Trenco, A.; Martínez, A. *Catal. Today* **2013**, *215*, 152−161.
(35) Liao, F.; Huang, Y.; Ge, J.; Zheng, W.; Tedsree, K.; Collier, P.; Hong, X.; Tsang, S. C. *Angew. Chem., Int. Ed.* **2011**, *50*, 2162−2165.
(36) Grandjean, D.; Pelipenko, V.; Batyrev, E. D.; van den Heuvel, J. C.; Khassin, A. A.; Yurieva, T. M.; Weckhuysen, B. M. *J. Phys. Chem. C* **2011**, *115*, 20175−20191.
(37) Kuld, S.; Conradsen, C.; Moses, P. G.; Chorkendorff, I.; Sehested, J. *Angew. Chem., Int. Ed.* **2014**, *53*, 5941−5945.
(38) Schott, V.; Oberhofer, H.; Birkner, A.; Xu, M.; Wang, Y.; Muhler, M.; Reuter, K.; Wöll, C. *Angew. Chem., Int. Ed.* **2013**, *52*, 11925−11929.
(39) Studt, F.; Sharafutdinov, I.; Abild-Pedersen, F.; Elkjær, C. F.; Hummelshøj, J. S.; Dahl, S.; Chorkendorff, I.; Nørskov, J. K. *Nat. Chem.* **2014**, *6*, 320−324.
(40) Herman, R. G.; Klier, K.; Simmons, G. W.; Finn, B. P.; Bulko, J. B.; Kobylinski, T. P. *J. Catal.* **1979**, *56*, 407−429.

DOI: 10.1021/acscatal.5b00877
ACS Catal. 2015, 5, 5607−5616

(41) Rasmussen, B. S.; Højlund Nielsen, L. P.; Villadsen, J.; Hansen, J. B. In *Studies in Surface Science and Catalysis*; Delmon, B.; Grange, P.; Jacobs, P. A.; Poncelet, G., Eds.; Elsevier: Amsterdam, 1987; Vol. *31*, pp 785−794.
(42) Fiedler, E.; Grossmann, G.; Kersebohm, D. B.; Weiss, G.; Witte, C. In *Ullmann's Encyclopedia of Industrial Chemistry*, 7th ed.; Elvers, B., Ed.; Wiley-VCH Verlag GmbH & Co. KGaA: Weinheim, 2012; Vol. *23*, pp 25−48.
(43) Gervasini, A.; Bennici, S. *Appl. Catal., A* **2005**, *281*, 199−205.
(44) Karelovic, A.; Ruiz, P. *Catal. Sci. Technol.* **2015**, *5*, 869−881.
(45) Studt, F.; Behrens, M.; Kunkes, E. L.; Thomas, N.; Zander, S.; Tarasov, A.; Schumann, J.; Frei, E.; Varley, J. B.; Abild-Pedersen, F.; Nørskov, J. K.; Schlögl, R. *ChemCatChem* **2015**, *7*, 1105−1111.
(46) Liu, G.; Willcox, D.; Garland, M.; Kung, H. H. *J. Catal.* **1984**, *90*, 139−146.
(47) Waugh, K. C. *Catal. Lett.* **2012**, *142*, 1153−1166.
(48) Natesakhawat, S.; Lekse, J. W.; Baltrus, J. P.; Ohodnicki, P. R.; Howard, B. H.; Deng, X.; Matranga, C. *ACS Catal.* **2012**, *2*, 1667−1676.
(49) Baltes, C.; Vukojević, S.; Schüth, F. *J. Catal.* **2008**, *258*, 334−344.
(50) Le Valant, A.; Comminges, C.; Tisseraud, C.; Canaff, C.; Pinard, L.; Pouilloux, Y. *J. Catal.* **2015**, *324*, 41−49.
(51) Lunkenbein, T.; Schumann, J.; Behrens, M.; Schlögl, R.; Willinger, M. G. *Angew. Chem., Int. Ed.* **2015**, *54*, 4544−4548.
(52) Nakamura, J.; Choi, Y.; Fujitani, T. *Top. Catal.* **2003**, *22*, 277−285.
(53) Kunkes, E. L.; Studt, F.; Abild-Pedersen, F.; Schlögl, R.; Behrens, M. *J. Catal.* **2015**, *328*, 43−48.
(54) Ostrovskii, V. E. *Catal. Today* **2002**, *77*, 141−160.
(55) Frost, J. C. *Nature* **1988**, *334*, 577−580.
(56) Calaza, F.; Stiehler, C.; Fujimori, Y.; Sterrer, M.; Beeg, S.; Ruiz-Oses, M.; Nilius, N.; Heyde, M.; Parviainen, T.; Honkala, K.; Häkkinen, H.; Freund, H.-J. *Angew. Chem., Int. Ed.* **2015**.
(57) Spencer, M. S. *Top. Catal.* **1999**, *8*, 259−266.
(58) Topsøe, N.-Y.; Topsøe, H. *Top. Catal.* **1999**, *8*, 267−270.
(59) Kandemir, T.; Girgsdies, F.; Hansen, T. C.; Liss, K.-D.; Kasatkin, I.; Kunkes, E. L.; Wowsnick, G.; Jacobsen, N.; Schlögl, R.; Behrens, M. *Angew. Chem., Int. Ed.* **2013**, *52*, 5166−5170.
(60) Samson, K.; Śliwa, M.; Socha, R. P.; Góra-Marek, K.; Mucha, D.; Rutkowska-Zbik, D.; Paul, J.-F.; Ruggiero-Mikołajczyk, M.; Grabowski, R.; Słoczyński, J. *ACS Catal.* **2014**, *4*, 3730−3741.
(61) Graciani, J.; Mudiyanselage, K.; Xu, F.; Baber, A. E.; Evans, J.; Senanayake, S. D.; Stacchiola, D. J.; Liu, P.; Hrbek, J.; Sanz, J. F.; Rodriguez, J. A. *Science* **2014**, *345*, 546−550.
(62) Van de Walle, C. G. *Phys. Rev. Lett.* **2000**, *85*, 1012−1015.
(63) Hartadi, Y.; Widmann, D.; Behm, R. J. *ChemSusChem* **2015**, *8*, 456−465.
(64) Pasupulety, N.; Driss, H.; Alhamed, Y. A.; Alzahrani, A. A.; Daous, M. A.; Petrov, L. *Appl. Catal., A* **2015**, DOI: 10.1016/j.apcata.2015.01.036.
(65) Bansode, A.; Urakawa, A. *J. Catal.* **2014**, *309*, 66−70.

DOI: 10.1021/acscatal.5b00877
ACS Catal. 2015, 5, 5607−5616